Algorithms for Stylus Instruments to Measure Aspheric Surfaces

CHANG-OCK LEE * KILSU PARK * BYONG CHON PARK †
YOON WOO LEE‡

Abstract

A reliable algorithm is developed for the analysis of the machined aspheric surfaces with a stylus instrument. This research has been done prior to the evaluation of uncertainties in the aspheric surface analysis. The algorithm considers two factors: the pickup configuration(pivoted arm) and the stylus radius. It also compensates for the sample tilt and the axis offset(the setup error) in the best-fit least squares process. The algorithm consists of two parts for instrument calibration and aspheric surface analysis, and has been coded by means of C++ and MATLAB. Further it was also applied to the instrument calibration and the aspheric surface measurement, and the results were compared with the instrument-produced ones. The developed algorithm shows better performance over the commercial instrument in both the instrument-calibration and the analysis of aspheric surfaces. Besides the uncertainty analysis, the developed algorithm will be a basis for the applications that the commercial instruments cannot provide with its own built-in code.

Keywords: aspheric surface, asphere, stylus instrument, pivoted arm.

1 Introduction

Stylus profilometry is a common approach for testing aspheric surfaces during the stage of generation and grinding in the manufacture of aspheric surfaces. It is simple, accurate and relatively low costly, although slow and of low resolution compared with the interferometer. The accuracy of the profilometry, however, is limited by many factors which include the transducer gain, surface texture, surface slope, mechanical way bend, blow or ripple of the stage guide, accumulated encoder/indexer errors, and so on. The accuracy of the profilometry is important because the removal rates are much higher in the generation and grinding than in the polishing. Often it is the last evaluation of the manufactured aspheric surface when the last process is diamond-turning or grinding. Therefore, it is worth evaluating the uncertainties of the aspheric surface measurement with a stylus instrument.

The code itself, due to the approximations or assumptions taken, contributes to the resultant uncertainties. Either the imperfection of the instrument functions or the incomplete knowledge

*Division of Applied Mathematics, KAIST, Daejeon, 305-701, Korea
†Division of Optical Metrology, KRISS, Daejeon, 305-340, Korea. E-mail: bcpark@kriss.re.kr
‡Division of Optical Metrology, KRISS, Daejeon, 305-340, Korea

about the metrological factors of the instrument, adds to the uncertainty budget, after the propagation through the execution of the algorithm. Unfortunately, however, the algorithm is not available since it is a 'black-box' in the commercial instrument. Furthermore, the relevant references are so restricted as far as the authors can find.

As the first step for the uncertainty analysis, this research is initiated with the focus on the development of algorithm that can be used in calibration and analysis instead of the 'black-box' in the instrument. Another objective is to modify the algorithm for the diverse application that the commercial instrument does not provide with the built-in code in the instrument. The research includes the development of the algorithm, coding with Visual C++ and MATLAB, the evaluation of the code with the simulated profile, and finally the demonstration of the actual calibration of the instrument, and then the measurement of an aspheric sample.

In section 2 the descriptions are given on the standard spheres and the aspheric surface, and the stylus instrument for measuring them. Section 3 deals with the structure of the algorithm and the role of its components. The part for instrument calibration(CAG) is the crucial one, which directly affects the accuracy of the profile coordinate. All of the four kinds of CAGs contrived are treated here for intercomparison in order to illuminate the considerations taken in the finally chosen CAG(CAG4). In section 4 the developed algorithm is evaluated by means of the generated profile as well as the actual surfaces. For the check of the algorithm we apply it to a raw profile generated by mathematical formula for a designed profile and find that we can re-construct the designed profile within the acceptable error. The uncertainty estimation in the aspheric surface measurement, based on the developed algorithm, is discussed in the final section.

2 Materials

Three kinds of standard balls are used for the instrument calibration with the radius $R = 80.034\,mm$, $21.9973\,mm$ and $12.4914\,mm$. An aspheric sample is made of aluminium and diamond-turned. Parameters for the manufacture are $R = -800\,mm$, $K = -0.843788$, $D_4 = 0.483902\text{E-}09$, $D_6 = -0.413819\text{E-}12$, $D_8 = 0.164575\text{E-}15$, $D_{10} = -0.234814\text{E-}19$, while other D_i's are all zero in the aspheric form described later. Then it is coated with the MaF_2 film for the protection of the fragile machined-aluminium surface.

Form Talysurf(FTS) series 2(Taylor Hobson, UK) is used for the aspheric surface measurement. It uses the laser pickup with the pivoted stylus arm. The range/resolution is $6\,mm/10\,nm$. The stylus arm is L-shaped, whose length is $12\,mm$ from the pivot to the edged corner and $6\,mm$ from the corner to the tip. The radius r of the stylus tip is $2\,\mu m$. These factors are used as parameters or starting values for the calibration as well as the aspheric surface measurement.

3 Development of Algorithms

3.1 Principle of the instrument calibration

As the transducer moves in x-axis direction, the data measured is distorted due to the arcuate movement of the stylus arm in z-axis direction. In order to correct the data to be the designed profile, the instrument does the calibration with the standard ball of radius known exactly. We first analyze the calibration process under some assumptions for the system to develop the algorithm. The calibration is eventually related to how we reconstruct the designed profile from the raw profile

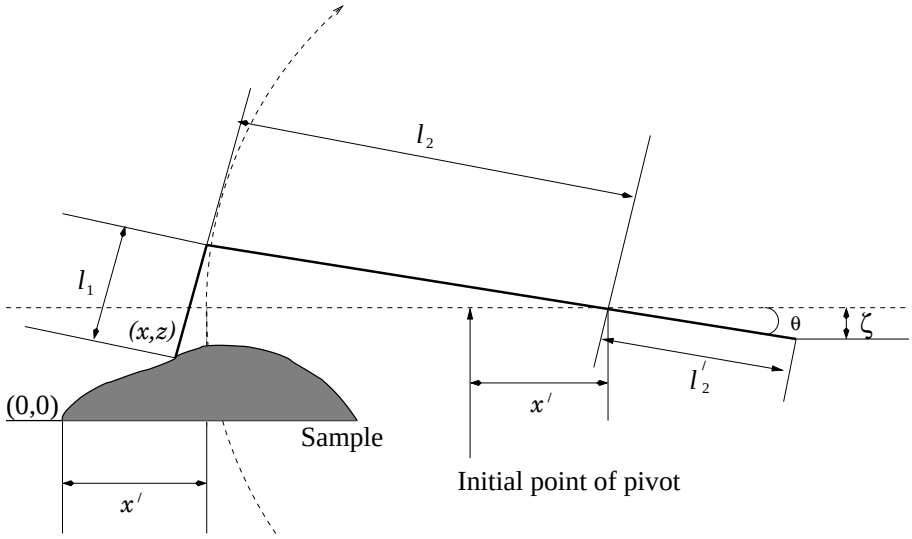

Figure 1: Geometry of the pickup configuration

distorted by various factors. Our concern is to know what the reconstruction process is. We model the calibration process with some assumptions:

- The arrangement of the pivoted stylus arm is perpendicular.
- The pivot position is fixed.
- The pivot angle is obtained exactly by the laser interferometer.

Figure 1 shows the geometry of the pickup configuration when the measurement is made. As the stylus transducer travels to x' in x-axis direction, the stylus moves arcuately about the pivot by θ in z-axis direction due to the pickup configuration, which causes the positional error with true locus (x, z) other than (x', z') obtained. Here it is assumed that the displacement of the stylus tip z' is computed by multiplying the displacement of the rear ζ by a constant K, say,

$$z' = K\frac{l_2}{l'_2}\,\zeta = Kl_2 \sin\theta. \tag{3.1}$$

When the stylus tip is of radius zero, we can derive the relation between the true locus of the stylus and the distorted raw data. From Figure 2, we have

$$\begin{aligned} \overline{AD} &= l_2 \tan\theta, \\ \overline{DE} &= l_1 - l_2 \tan\theta. \end{aligned}$$

Hence it follows that

$$\begin{aligned} \overline{HE} &= \overline{DE}\cos\theta \\ &= (l_1 - l_2 \tan\theta)\cos\theta \\ &= l_1 \cos\theta - l_2 \sin\theta. \end{aligned}$$

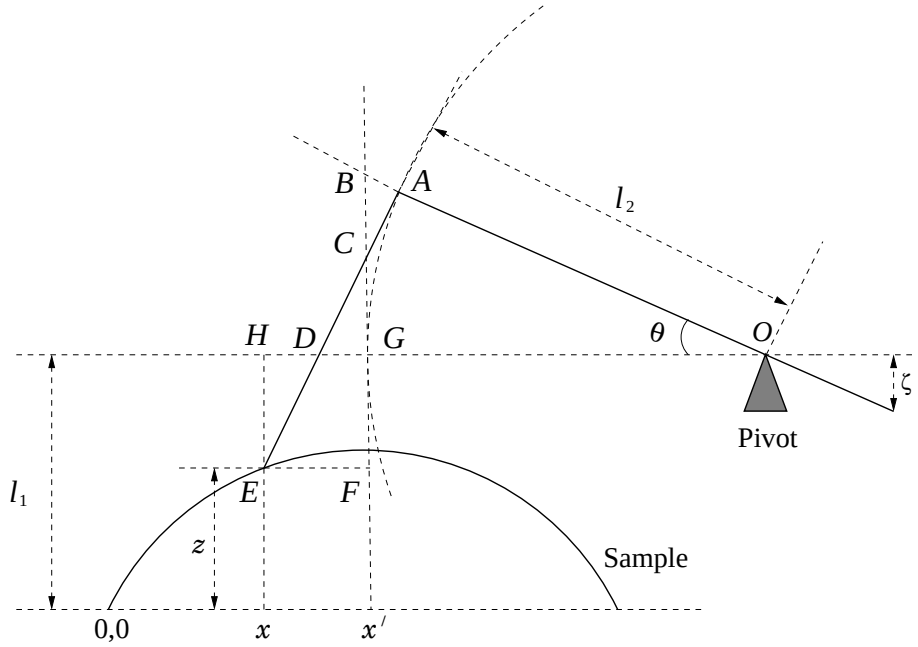

Figure 2: Specified model of the pickup configuration

Thus we get

$$\begin{aligned} z &= l_1 - \overline{HE} \\ &= l_1(1-\cos\theta) + l_2\sin\theta. \end{aligned} \tag{3.2}$$

Furthermore, we have

$$\begin{aligned} \overline{AB} &= \overline{OB} - \overline{OA} = \frac{l_2}{\cos\theta} - l_2 = l_2\left(\frac{1-\cos\theta}{\cos\theta}\right), \\ \overline{DG} &= \overline{CD}\sin\theta, \\ \overline{CE} &= l_1 - \overline{AC} = l_1 - \frac{\overline{AB}}{\tan\theta}. \end{aligned}$$

In ΔCEF and ΔCDG, using the ratio $\overline{CD} : \overline{CE} = \overline{DG} : \overline{EF}$, we have

$$\begin{aligned} \overline{EF} = x' - x &= \frac{\overline{CE}\,\overline{DG}}{\overline{CD}} \\ &= \overline{CE}\sin\theta \\ &= \left(l_1 - \frac{\overline{AB}}{\tan\theta}\right)\sin\theta. \end{aligned}$$

Hence we get

$$\Delta x = x - x' = l_2(1-\cos\theta) - l_1\sin\theta. \tag{3.3}$$

Using the relations (3.2) and (3.3) we can reconstruct the designed profile (x, z) from the raw data (x', z') if above assumptions hold and other factors are ignored. The manual of the FTS [1] and Stevens [2] suggest other compensation relation instead of (3.2) and (3.3), which is the polynomial relation between the true locus and the raw profile. The relation is

$$z = A_1 z' + A_2 z'^2 + A_3 z'^3 + A_4 z'^4, \tag{3.4}$$

$$\Delta x = x - x' = B_1 z' + B_2 z'^2 + B_3 z'^3, \tag{3.5}$$

where $A_1, \cdots, B_1, \cdots$ are computed by the calibration algorithm using 100 raw data points. By substituting (3.1) for (3.2) and (3.3) we obtain the Talyor expansion as

$$z = \frac{l_2}{L_2} z' + \frac{l_1}{2{L_2}^2} z'^2 + \frac{l_1}{8{L_2}^4} z'^4 + \cdots, \tag{3.6}$$

$$\Delta x = x - x' = -\frac{l_1}{L_2} z' + \frac{l_2}{2{L_2}^2} z'^2 + \frac{l_2}{8{L_2}^4} z'^4 + \cdots, \tag{3.7}$$

where $L_2 = K l_2$, which are similar to (3.4) and (3.5). There are, however, some obstacles which do not allow to use the relations (3.6) and (3.7) directly for the compensation. The actual tip of the stylus is of nonzero radius r and the dimensions like l_1, l_2 are just nominal values, not exact. In this research we assume that the stylus tip radius r is $0.002\,mm$. Moreover the arrangement of the stylus arm may not be perpendicular. Due to these reasons, instead of using (3.6) and (3.7), we develop an algorithm to compute the constants in (3.4) and (3.5).

3.2 Principle of aspheric surface analysis

An aspheric surface is given from a basic conic section with a superimposed symmetric deviation. The deviation can be described by a symmetrical polynomial expression. The mathematical expression of an aspheric form is

$$z = \frac{x^2}{R + \sqrt{R^2 - (1+K)x^2}} + D_1|x| + D_2|x|^2 + \cdots + D_{12}|x|^{12}, \tag{3.8}$$

where x is the horizontal distance from the aspheric axis and z is the corresponding vertical distance. The base radius of curvature of the conic section is R, which has $(+)$ value for convex base and $(-)$ value for concave base. The conic constant K is as below:

$K < -1$: Hyperboloid,
$K = -1$: Paraboloid,
$-1 < K < 0$: Ellipsoid,
$K = 0$: Sphere,
$K > 0$: Oblate Ellipsoid.

Above equation for an aspheric surface is first fitted to the measured profile using the best least squares fitting with the given radius R and aspheric coefficients D_i's. Since the setup error contributes to the tilt and the dual axis shift, we have to consider these effects in the least squares fitting. Then we get the residuals by calculating the distance between the actual profile and the absolute aspheric form.

3.3 An algorithm for the profile of the standard ball: CAG1

From the distorted raw profile obtained by measuring the standard ball of radius R we take the minimization process which will give a minimizer that becomes the calibration constants. Let (x', z') be the raw data. If $A_1, \cdots, B_1 \cdots$ are calibration constants, we can get the compensated (x, z), which is different from the designed profile, by the relations (3.4) and (3.5). Considering the least squares circle fitting to the compensated data (x, z), we get the radius $\tilde{R}$ of the circle and then compare $\tilde{R}$ with the radius R of the standard ball. Thus our first calibration algorithm is focused on the minimization of the difference $|R - \tilde{R}|$. In other words, we want to find the calibration constants $(A_1, \cdots, B_1, \cdots)$ which will therefore minimize the difference $|R - \tilde{R}|$. In the whole process we use 100 points from the raw data as the FTS does.

We set up the following formulation.

$$F(A_1, \cdots, B_1, \cdots) = \min_{\tilde{R}} F = \min_{\tilde{R}} |R - \tilde{R}|^2, \tag{3.9}$$

where $(\tilde{a}, \tilde{b}, \tilde{R})$= argmin $G(a, b, d)$,

$$\begin{aligned} G &= \sum_{i=1}^{N} (\sqrt{(x_i - a)^2 + (z_i - b)^2} - d)^2, \\ d &= \frac{\sum_{i=1}^{N} \sqrt{(x_i - a)^2 + (z_i - b)^2}}{N}. \end{aligned}$$

Here, N is the number of selected raw data (x'_i, z'_i). We describe the algorithm step by step.

1. Take an initial guess for a minimizer $(A_1, \cdots, B_1, \cdots)$.
2. Do compensate the raw data with (3.4) and (3.5).
3. Find the least square circle of radius $\tilde{R}$ centered at $(\tilde{a}, \tilde{b})$ fitting the compensated data.
4. Update $(A_1, \cdots, B_1, \cdots)$ so that $|R - \tilde{R}|^2$ decreases.

In the third step we use the exact formula for the least squares circle which is given in Appendix. To implement the step 4 we use the Nelder-Mead simplex method [3]. The quasi-Newton method for minimizing nonlinear multi variable function can be available. But since it requires the computation of derivatives and our function F is not easily expressed explicitly with respect to $A_1, \cdots, B_1, \cdots$, it is not adequate to use the quasi-Newton method for our algorithm. The Nelder-Mead simplex method, on the other hand, minimizes a scalar-valued nonlinear function of multi variables using only function evaluations, without any derivative information. The Nelder-Mead method falls in the general class of *direct search methods*, which maintain at each step a nondegenerate n-dimensional *simplex* that is a convex hull of $n + 1$ vertices. Each iteration of the method begins with a simplex, specified by its $n + 1$ vertices and the associated function values. One or more test vertices are computed, along with their function values, and the iteration terminates with a new different simplex when the function values at its vertices satisfy the stop condition. For more detail see [4].

Once the calibration algorithm is completed, by using the computed calibration constants we apply (3.4) and (3.5) to compensate the raw profile (x'_i, z'_i). Among the compensated data we select $2,000$ points and calculate the radius $\tilde{R}$ of the least squares circle fit to these data. We also compute the form error which is the residual of the compensated data away from the least squares circle.

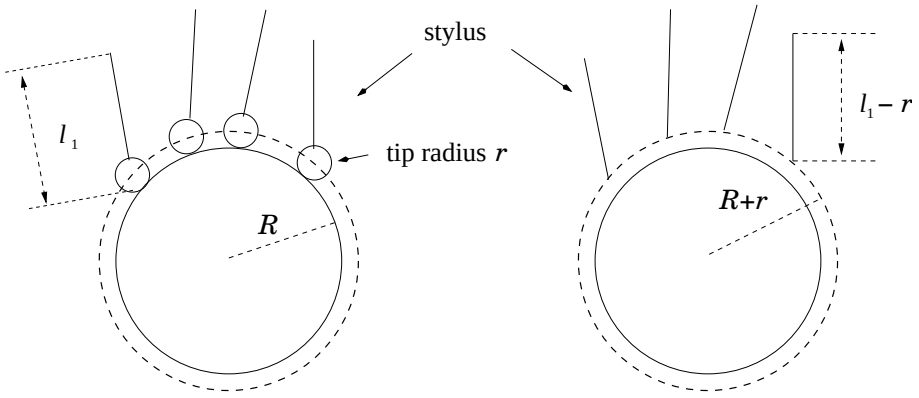

Figure 3: Measurement by the stylus tip of radius r(left) and of radius zero(right)

3.4 An algorithm for the convoluted profile of the standard ball: CAG2

We make a little modification on the target function F in (3.9). The idea is based on the following observation. When the measurement is made through the standard ball of radius R by the stylus of tip radius r, the obtained raw profile under the assumptions in section 3.1 is the same as that obtained from the measurement of the standard ball of radius $R + r$ by the stylus of tip radius zero. Figure 3 is the graphical description of two cases.

In section 3.3, we developed a compensation algorithm to adjust the raw data to the profile of the ball of radius R as a target profile. The strategy in this section, on the other hand, is that we first compensate the raw data to get the object profile of the standard ball of radius $R + r$ and then translate all of the data in normal direction at each point by r. Note that the center of the least squares circle is located in the normal direction. The final profile is eventually what we want to reconstruct from the raw profile. This work implies that we don't have to consider the stylus tip radius and its convolution with a surface, though these are main factors for the distorted raw profile, if we focus on the ball of enlarged radius and the stylus tip of radius zero. This means that we can get the modified relation between the raw data and the standard profile of radius $R + r$. That is, if we replace R with $R + r$ and l_1 with $l_1 - r$ in (3.2) and (3.3), we have

$$\begin{aligned} z &= l_2 \sin\theta + (l_1 - r)(1 - \cos\theta), \\ \Delta x = x - x' &= l_2(1 - \cos\theta) - (l_1 - r)\sin\theta. \end{aligned}$$

Using this compensation rule, we are able to reconstruct almost perfect object profile when the assumptions of the pickup configuration in section 3.1 hold.

Now in a modified algorithm for the calibration the function F becomes

$$F = |(R + r) - R^*|^2,$$

where $(\tilde{a}, \tilde{b}, R^*)$= argmin $G(a, b, d)$,

$$\begin{aligned} G &= \sum_{i=1}^{N} (\sqrt{(x_i - a)^2 + (z_i - b)^2} - d)^2, \\ d &= \frac{\sum_{i=1}^{N} \sqrt{(x_i - a)^2 + (z_i - b)^2}}{N}. \end{aligned}$$

Here, N is the number of the raw data (x_i', z_i'). We apply the same minimization tool, the Nelder-Mead simplex method, and the exact formula for the least squares circle in Appendix.

3.5 An improved algorithm for the profile of the standard ball: CAG3

So far we have concentrated on the minimization of the radius error which is the difference between the radius of the standard ball and that of the reconstructed profile. This strategy gives poorer results than the FTS does as far as the residual error is concerned and there exists a severe deviation in calibration constants which are what we want to find in the long run. Moreover the form errors show the significant differences.

In the manual of the FTS [1], we notice that the instrument measures dimensions, form and texture simultaneously. Dimensions such as radius, distance and angle are used to define the shape of a surface, while form is deviation away from the intended nominal shape of the surface. In our research we pay little attention to the texture such as waviness and roughness which are related to the undesired machine tool effect. Up to now we have missed the form of a surface in modelling a calibration algorithm. With this fact in mind we add the form error term to the minimization function F, which is also to be minimized with the difference of radius. Then the function F becomes

$$\begin{aligned} F(A_1, \cdots, B_1, \cdots) &= \min_{(\tilde{a}, \tilde{b}, \tilde{R})} F \\ &= \min_{(\tilde{a}, \tilde{b}, \tilde{R})} \left(\varepsilon N |R - \tilde{R}|^2 + \sum_{i=1}^{N} \left(\sqrt{(x_i - \tilde{a})^2 + (z_i - \tilde{b})^2} - \tilde{R} \right)^2 \right). \end{aligned}$$

Here (x_i, z_i) are the compensated data for the raw data (x_i', z_i') using the following relation

$$\begin{aligned} z_i &= A_1 z_i' + A_2 {z_i'}^2 + A_3 {z_i'}^3 + A_4 {z_i'}^4, \\ \Delta x_i = x_i - x_i' &= B_1 z_i' + B_2 {z_i'}^2 + B_3 {z_i'}^3, \end{aligned}$$

where $(A_1, \cdots, B_1, \cdots)$ is determined by the Nelder-Mead method as in previous algorithms and $(\tilde{a}, \tilde{b})$ and $\tilde{R}$ are the center and the radius of the least squares circle, respectively, fitting the data (x_i, z_i) which is computed directly by the exact formula for the least square circle. The first term and second term in the function F are related to dimensions and the form of the surface, respectively. We introduce the weight parameter ε for the balance between two terms and its optimal value is determined by experiments.

3.6 An improved algorithm for the convoluted profile of the standard ball: CAG4

As in section 3.4 if we replace R with $R+r$ in the function F in section 3.5 we get a new calibration algorithm which eventually gives more improved results rather than previous ones. We already

knew the fact that whether measured by the stylus of tip radius r through the standard ball of radius R or measured by the stylus of zero radius through the standard ball of enlarged radius $R+r$, both raw profiles are the same (Figure 3). Thus once the raw profile is compensated to give the data which is intended to be the circle of radius $R+r$, we translate the compensated data by the tip radius r in the normal direction at each point and finally get the designed profile. The function F in section 3.4, of course, must be changed to include dimensions and the form of the surface, standard ball of radius $R+r$. That is,

$$F = \varepsilon N|(R+r) - R^*|^2 + \sum_{i=1}^{N} \left(\sqrt{(x_i - \tilde{a})^2 + (z_i - \tilde{b})^2} - R^* \right)^2,$$

where r is the tip radius of the stylus and R^* is the radius of the optimized circle centered at $(\tilde{a}, \tilde{b})$ to the translated data expected to be the circle of radius $R+r$. We also introduce the weight parameter ε as in section 3.5 which is determined by experiments.

3.7 Aspheric analysis algorithm: AAG

When the measurement of an aspheric surface is made, we first correct the obtained raw profile using the polynomial expansions whose coefficients are calculated by the calibration algorithm CAG4. Since the set up error causes the tilt and the dual-axis shift in the measurement, we have to compensate the corrected data for these effects by the minimization process so that the best least squares fit of the data to the designed aspheric surface is obtained. The best least squares fit is obtained by applying the effects of tilt and axes shift to the corrected data and then the residuals, the distance between the best least squares fit and the corrected data parallel to the aspheric axis are calculated.

Let (x_i', z_i') be the corrected data and (θ, X, Z) the tilt and the dual-axis shift to be determined. Then we find (θ, X, Z) by the best least squares fit of the corrected data to the given aspheric form of radius R, conic constant K, aspheric coefficients D_i's. Such a process can be done by minimizing the function

$$F(\theta, X, Z) = \sum_{i=1}^{N} \left(z_i - \frac{{x_i}^2}{R + \sqrt{R^2 - (1+K){x_i}^2}} + D_1|x_i| + \cdots + D_{12}|x_i|^{12} \right)^2$$

where (x_i, z_i) is the data obtained by compensation of (x_i', z_i') for the tilt and the axes shift and hence depends on (θ, X, Z). That is ,

$$\begin{aligned} \mathrm{rotx} &= \cos\theta\, x_i' + \sin\theta\, z_i', \\ \mathrm{rotz} &= -\sin\theta\, x_i' + \cos\theta\, z_i', \\ x_i &= \mathrm{rotx} + X, \\ z_i &= \mathrm{rotz} + Z. \end{aligned}$$

We use the Nelder-Mead simplex method for this minimization with some modification for the arguments of the function F. Since the effect of each argument of F varies in the magnitude, we make balances between them by introducing weights. The weights are computed by considering the slope of the function F with respect to each argument. By restricting the behavior of the simplex by means of these weights we can prevent the simplex from proceeding one way too excessively.

	A_1	A_2	A_3	A_4	B_1	B_2	B_3
FTS	9.919971E-1	2.158609E-3	8.936630E-6	0E+0	-2.099870E-1	8.758166E-3	1.508436E-5
CAG1	9.921919E-1	1.671672E-3	4.220102E-5	1.136036E-7	-2.015635E-1	8.066763E-3	5.017382E-5
CAG2	9.921906E-1	1.667328E-3	3.691162E-5	1.135026E-7	-2.017304E-1	8.039227E-3	8.014337E-5
CAG3	9.920358E-1	2.139428E-3	6.621414E-6	8.515906E-8	-2.079629E-1	8.059897E-3	-3.420779E-5
CAG4	9.920139E-1	2.142083E-3	5.008175E-6	7.307620E-8	-2.080658E-1	8.093072E-3	-6.657344E-6

Table 1: Calibration constants for the FTS and our algorithms for $R = 80.034\,mm$.

	$\tilde{R}$	$\lvert R - \tilde{R}\rvert$	Form error
FTS	8.003472E+1	7.193198E-4	1.487352E-1
CAG1	8.003754E+1	3.539471E-3	4.610732E-1
CAG2	8.003758E+1	3.578797E-3	4.599086E-1
CAG3	8.003399E+1	1.130575E-5	5.148918E-3
CAG4	8.003403E+1	3.051405E-5	3.793643E-3

Table 2: Radius errors and form errors from the FTS and our algorithm for $R = 80.034\,mm$.

We take the second derivative as the weights by observing that the function F is similar as the polynomial of degree 2 with respect to each argument.

If the residual error is convex/concave, which is due to the superimposed radius, then we increase/decrease the radius and repeat the process to get the residual error closest to the straight line. To analyze the aspheric surface, some parameters are calculated, for example, Rt, Tilt, etc.

4 Numerical Results

4.1 Calibration algorithms: CAG1-CAG4

We demonstrate the performance of our calibration algorithms by applying them to the several standard balls. To compare the results between the instrument calibration and our algorithms, we provide the calibration constants, the radius error and the form error. For each radius error and form error, we compensate the raw profile using the computed calibration constants and then do the least squares circle fitting of the selected $2,000$ data to get the optimized circle. Then we calculate the radius error between the optimized circle of radius $\tilde{R}$ and the standard ball of radius R, and the form error which is the difference between the optimized circle and the compensated data.

Table 1, 3 and 5 show the calibration constants calculated by the instrument(FTS) and our algorithms CAG1-CAG4 for three standard balls. Table 2, 4 and 6 show the computed radius, the residual error and the form error. The algorithm CAG4 reveals an excellent performance with regard to the radius error and the form error. The calibration constants are almost close to those of the instrument in leading coefficients of the polynomial expansions though other ones are a little different. For the algorithms CAG2 and CAG4 we use $\varepsilon = 0.018$ for the optimal weight parameter obtained by experiment. In Figure 4 and 8 we illustrate the same results with histograms, from

	A_1	A_2	A_3	A_4	B_1	B_2	B_3
FTS	9.920103E-1	2.153160E-3	7.344784E-6	0E+0	-2.097281E-1	8.730486E-3	-2.523684E-6
CAG1	9.922496E-1	1.662017E-3	1.222852E-4	1.127281E-7	-2.014693E-1	8.311278E-3	-1.031809E-4
CAG2	9.922236E-1	1.657553E-3	9.463904E-5	1.133155E-7	-2.017460E-1	8.284536E-3	-6.097699E-5
CAG3	9.922381E-1	2.003917E-3	-8.750913E-6	6.923027E-8	-2.069862E-1	7.548488E-3	-4.491470E-4
CAG4	9.920199E-1	2.146257E-3	4.699312E-8	8.323336E-8	-2.079875E-1	8.138837E-3	2.077047E-5

Table 3: Calibration constants for the FTS and our algorithms for $R = 21.9973\,mm$.

	$\tilde{R}$	$\lvert R - \tilde{R}\rvert$	Form error
FTS	2.199709E+1	2.090294E-4	2.861110E-1
CAG1	2.199835E+1	1.049986E-3	7.844832E-1
CAG2	2.199836E+1	1.062738E-3	7.650703E-1
CAG3	2.199739E+1	9.098338E-4	9.691462E-2
CAG4	2.199730E+1	3.253492E-6	6.721325E-3

Table 4: Radius errors and form errors from the FTS and our algorithm for $R = 21.9973\,mm$.

which it is clear that the algorithm CAG4 results in the smallest radius error and the form error among four algorithms. Table 7 shows the results when the algorithm CAG4 is applied to the computer-generated data of radius $R = 80.034\,mm$ according to the mathematical formula for the sphere to avoid noises caused by the instrument. This illustrates again the superiority of the algorithm CAG4.

4.2 Aspheric analysis algorithm: AAG

We measure the aspheric surface whose parameters are $R = -800\,mm$, $K = -0.843788$, and aspheric coefficients $D_4 = 0.483902\text{E-}09$, $D_6 = -0.413819\text{E-}12$, $D_8 = 0.164575\text{E-}15$, $D_{10} = -0.234814\text{E-}19$, while other D_i's are all zero in the aspheric form in (3.8). When the data is analyzed by the instrument, the parameters are calculated as $R = -801\,mm$, Tilt = 0.4741 deg and Rt = 3.5287E-4 mm with the residual error shown in Figure 6, where Rt denotes the difference between the maximum peak and the valley. In order to compare this result with our algorithm, we compensate the profile with calibration constants computed by the algorithm CAG4 which shows the best performance. Using the algorithm AAG we analyze the data and obtain the radius R for which the residual error is closest to the flat line. We also calculate Rt and Tilt among the parameters. Figure 7 shows the residual error with the obtained radius $R = -801\,mm$, Tilt = 0.3269 deg and Rt = 2.9504E-4 mm. We get the similar residual profile to the instrument and in addition smaller Rt than with the instrument. For the check of our algorithm, we generate a designed profile according to the formula (3.8) of the aspheric surface which has the same parameters as above and then apply the algorithm to analyze it. Figure 5 illustrates that the residual error for the generated profile is much smaller and close to the straight line, compared with Figure 7. In this case the parameters calculated are $R = -800\,mm$, Tilt = 0.0018 deg and Rt = 9.6249E-6 mm.

	A_1	A_2	A_3	A_4	B_1	B_2	B_3
FTS	9.922618E-1	2.129955E-3	-8.455489E-5	0E+0	-2.095993E-1	8.553904E-3	-4.655429E-4
CAG1	9.926017E-1	1.685148E-3	1.284871E-4	1.120399E-7	-2.037717E-1	8.107244E-3	-7.300719E-5
CAG2	9.924143E-1	1.676170E-3	1.311835E-4	1.121029E-7	-2.038728E-1	8.377395E-3	-2.315972E-4
CAG3	9.924458E-1	1.642765E-3	1.255581E-4	3.590116E-8	-2.076666E-1	8.414775E-3	-1.313433E-4
CAG4	9.922644E-1	2.176968E-3	-1.010215E-4	6.718874E-8	-2.077423E-1	7.833783E-3	-9.705298E-4

Table 5: Calibration constants for the FTS and our algorithms for $R = 12.4914\,mm$.

	$\tilde{R}$	$\lvert R - \tilde{R}\rvert$	Form error
FTS	1.249257E+1	1.171124E-3	4.229300E-2
CAG1	1.249164E+1	2.403388E-4	9.240607E-2
CAG2	1.249163E+1	2.338631E-4	8.790374E-2
CAG3	1.249159E+1	1.945279E-4	1.751542E-2
CAG4	1.249144E+1	4.188657E-5	4.271578E-3

Table 6: Radius errors and form errors from the FTS and our algorithm for $R = 12.4914\,mm$.

R	$\tilde{R}$	$\lvert R - \tilde{R}\rvert$	Form error
80.034	8.003465E+1	6.571151E-4	2.313677E-4
21.9973	2.199787E+1	5.789966E-4	5.331851E-4
12.4914	1.249157E+1	1.776835E-4	4.888169E-5

Table 7: Radius errors and form errors of CAG4 for the computer-generated data.

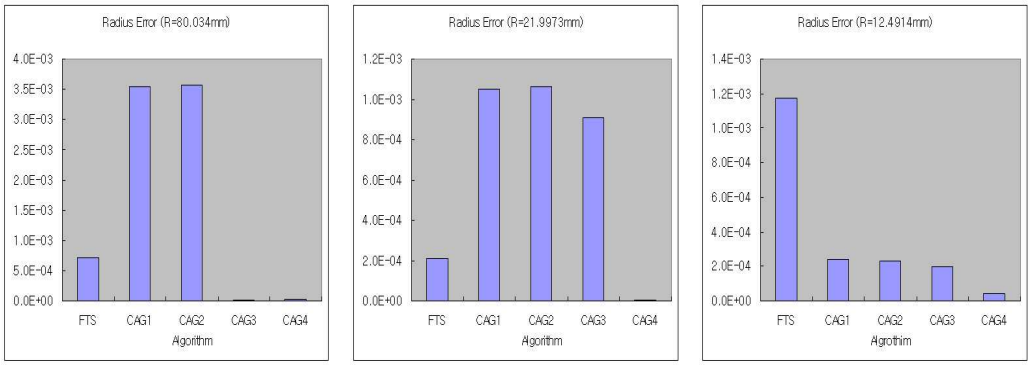

Figure 4: Radius error histograms for R=80.034, 21.9973 and 12.4914 mm with respect to our algorithms from left to right.

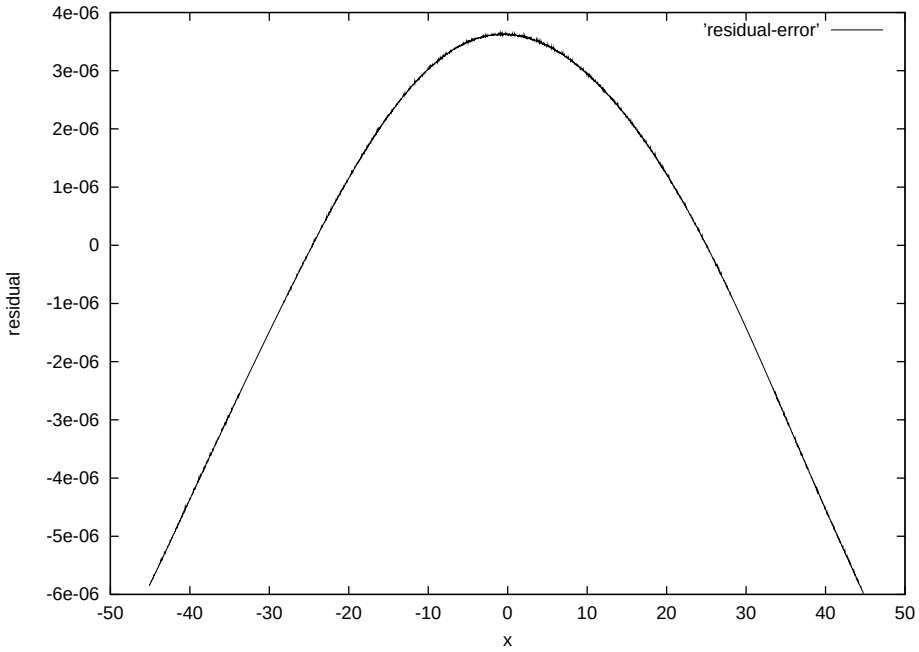

Figure 5: Residual error of AAG for the computer-generated data

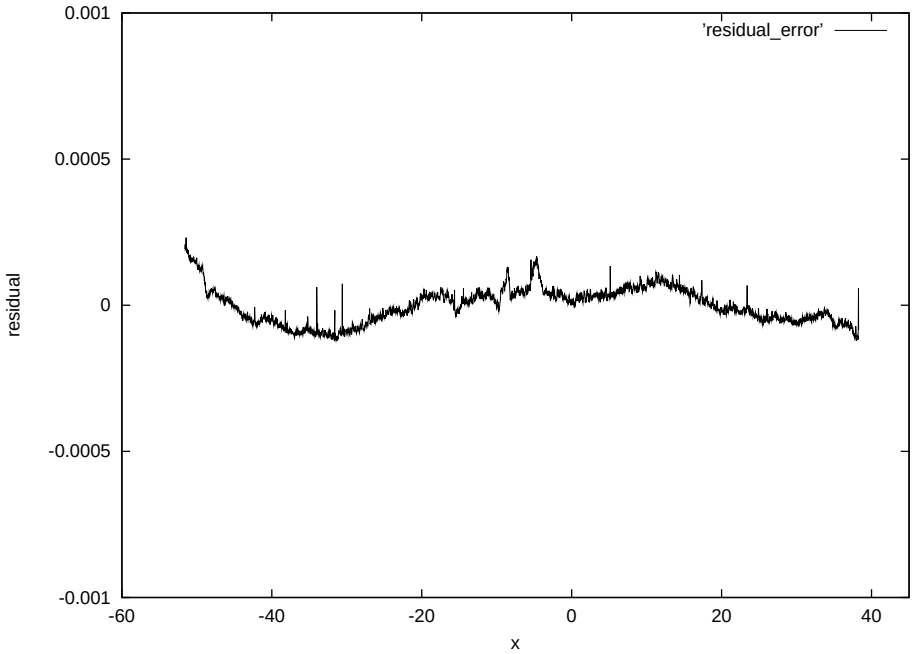

Figure 6: Residual error of the FTS for the measured profile

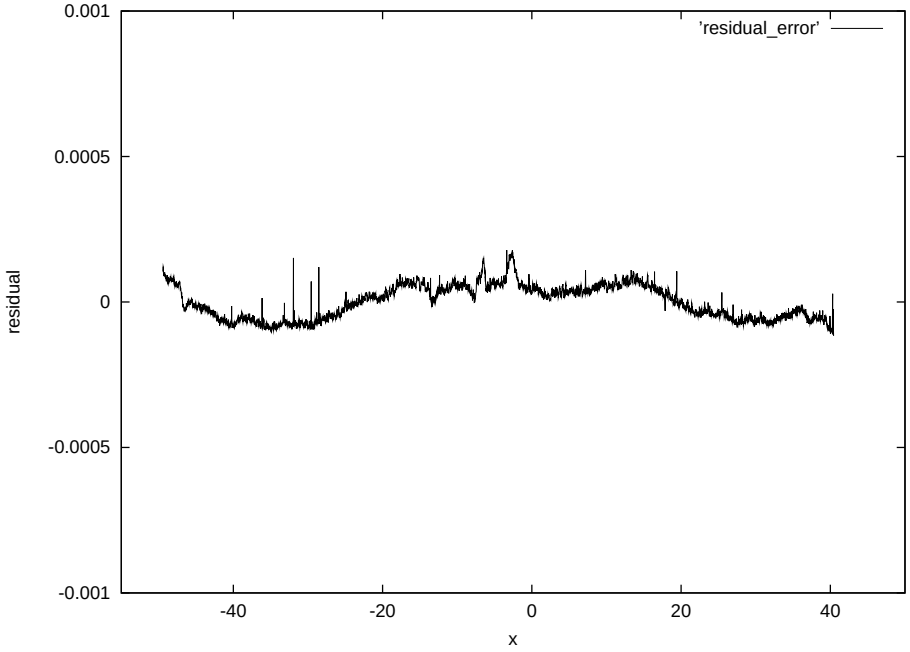

Figure 7: Residual error of AAG for the measured profile

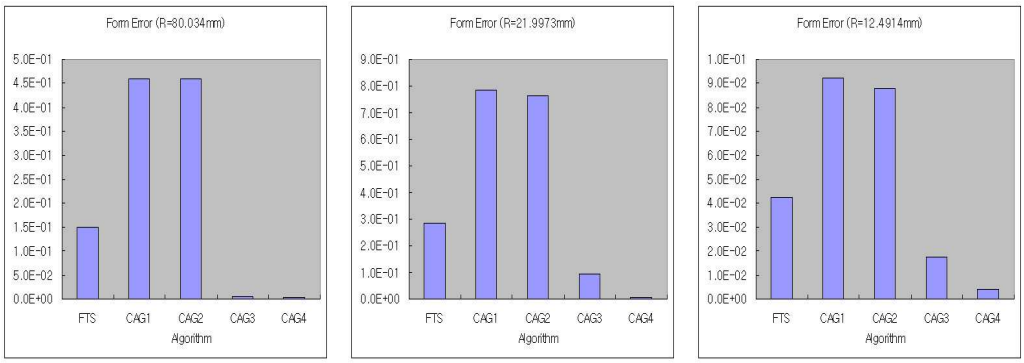

Figure 8: Form error histograms for R=80.034, 21.9973 and 12.4914 mm with respect to our algorithms from left to right.

5 Conclusions

A reliable algorithm has been developed for measurement of the aspheric surfaces with a stylus instrument. It was coded by means of C++ and MATLAB, and actually applied to the instrument calibration and the asphere analysis. The code shows better performance over the one built in the commercial instrument. An user-specific application which the commercial instrument does not provide, as well as the measurement uncertainty analysis, can be effectively performed with the developed algorithm.

Appendix: Exact Formula for the Least Squares Circle

We want to find a circle to optimize a given data (x_i, z_i). Let (a, b) be the center of the circle and r the radius. Then we minimize the function G given by

$$G(a,b,r) = \sum_{i=1}^{N} \left((x_i - a)^2 + (z_i - b)^2 - r^2 \right)^2 .$$

By taking derivatives of G with respect to a, b and r, we get

$$\frac{\partial G}{\partial a} = 4\sum_{i=1}^{N}[(x_i - a)^2 + (z_i - b)^2 - r^2](x_i - a) = 0, \tag{A.1}$$

$$\frac{\partial G}{\partial b} = 4\sum_{i=1}^{N}[(x_i - a)^2 + (z_i - b)^2 - r^2](x_i - b) = 0, \tag{A.2}$$

$$\frac{\partial G}{\partial r} = -4\sum_{i=1}^{N}[(x_i - a)^2 + (z_i - b)^2 - r^2]r = 0. \tag{A.3}$$

From (A.3), we have a relation with respect to r,

$$r^2 = \frac{1}{N}\sum_{i=1}^{N}[(x_i - a)^2 + (z_i - b)^2]. \tag{A.4}$$

To find the formula about a and b, expanding (A.3) gives

$$N(a^2 + b^2 - r^2) + \sum_{i=1}^{N}({x_i}^2 - 2ax_i + {z_i}^2 - 2bz_i) = 0. \tag{A.5}$$

From (A.1) and (A.2), using (A.3) and (A.5), we obtain

$$\sum_{i=1}^{N}[{x_i}^2 - 2ax_i + {z_i}^2 - 2bz_i](x_i - \bar{x}) = 0, \tag{A.6}$$

$$\sum_{i=1}^{N}[{x_i}^2 - 2ax_i + {z_i}^2 - 2bz_i](z_i - \bar{z}) = 0, \tag{A.7}$$

where

$$\bar{x} = \frac{\sum_{i=1}^{N} x_i}{N}, \quad \bar{z} = \frac{\sum_{i=1}^{N} z_i}{N}.$$

From (A.6) and (A.7), we have a system

$$\begin{pmatrix} 2\sum_{i=1}^{N} x_i(x_i - \bar{x}) & 2\sum_{i=1}^{N} z_i(x_i - \bar{x}) \\ 2\sum_{i=1}^{N} x_i(z_i - \bar{z}) & 2\sum_{i=1}^{N} z_i(z_i - \bar{z}) \end{pmatrix} \begin{pmatrix} a \\ b \end{pmatrix} = \begin{pmatrix} \sum_{i=1}^{N} ({x_i}^2 + {z_i}^2)(x_i - \bar{x}) \\ \sum_{i=1}^{N} ({x_i}^2 + {z_i}^2)(z_i - \bar{z}) \end{pmatrix}. \tag{A.8}$$

Solving this system, we obtain (a, b) and therefore r from (A.4).

Acknowlegement

This work was partially supported by the MOST-sponsored project "Study of evaluation technology for precision optical system", KRISS-to-university joint-research program and KRF-2002-070-C00004. The authors acknowledge Geon-Hee Kim of Korea Basic Science Institute for manufacturing an asphere sample.

References

[1] *The Form Talysurf Series 2 Operator's Handbook* (Rank Taylor Hobson Ltd).

[2] D. Stevens, "The Application of optical techniques in aspheric surface assessment", Int. J. Mach. Tools Manufact., 32, 19-25, (1992).

[3] J. A. Nelder and R. Mead, "Simplex method of function minimization", Comput. J., 7, 308-313, (1965).

[4] J. C. Lagarias, J. A. Reeds, M. H. Wright and P. E. Wright, "Convergence properties of the Nelder-Mead simplex method in low dimensions", SIAM J. Optim., 9, 112-147, (1998).